Available online at www.sciencedirect.com
ScienceDirect
Journal of Power Sources 163 (2007) 971–985
JOURNAL OF POWER SOURCES
www.elsevier.com/locate/jpowsour

Experimental investigation of fuel cell dynamic response and control

Keith A. Williams [a,*], Warren T. Keith [a], Michael J. Marcel [b], Timothy A. Haskew [b], W. Steve Shepard [a], Beth A. Todd [a]

[a] *Department of Mechanical Engineering, 290 Hardaway Hall, Box 870276, The University of Alabama, Tuscaloosa, AL 35487-0276, United States*
[b] *Department of Electrical and Computer Engineering, 317 Houser Hall, Box 870286, The University of Alabama Tuscaloosa, AL 35487-0286, United States*

Received 30 August 2006; received in revised form 30 September 2006; accepted 3 October 2006
Available online 15 November 2006

Abstract

An experimental study of the dynamic response of a commercial fuel cell system is presented in this work. The primary goal of the research is an examination of the feasibility for using fuel cells in a load-following mode for vehicular applications, where load-following implies that the fuel cell system provides the power necessary for transient responses without the use of additional energy storage elements, such as batteries or super-capacitors. The dynamic response of fuel cell systems used in the load-following mode may have implications for safe and efficient operation of vehicles. To that end, a DC–DC converter was used to port the power output of the fuel cell to a resistive load using a pulse-width-modulating circuit. Frequency responses of the system were evaluated at a variety of DC offsets and AC amplitudes of the PWM duty cycle from 1 out to 400 Hz. Open-loop transient responses are then evaluated using transitions from 10% to 90% duty cycle levels, followed by dwells at the 90% level and then transitions back to the 10% level. A classical proportional–integral controller was then developed and used to close the loop around the system, with the result that the fuel cell system was driven to track the same transient. The controller was then used to drive the fuel cell system according to a reference power signal, which was a scaled-down copy of the simulated power output from an internal combustion engine powering a conventional automobile through the Federal Urban Driving Schedule (FUDS). The results showed that the fuel cell system is capable of tracking transient signals with sufficient fidelity such that it should be applicable for use in a load-following mode for vehicular applications. The results also highlight important issues that must be addressed in considering vehicular applications of fuel cells, such as the power conditioning circuit efficiency and the effect of stack heating on the system response.

Keywords: Fuel cells; Dynamic response; Fuel cell vehicles

1. Introduction

It is generally accepted that fuel cells have the potential for being a primary power source in automobiles. A number of technical issues remain before widespread fuel cell use can be realized, including reducing the capital cost of the fuel cell systems and improving hydrogen storage. Another important issue is determining the most appropriate way to utilize the fuel cell power plant. For example, it may be appropriate to utilize the fuel cell system as a mobile battery charger, such that the fuel cell is essentially a range-extender for what may be a plug-in electric vehicle. Alternatively, it may be that the fuel cell system may be the dominant source of power for the drivetrain, with batteries or other auxiliary energy sources used only for fuel cell system startup and shutdown. There is then a continuum of implementation approaches between those two extremes, where fuel cells and other electrical energy sources are more or less dominant powerplants in a given vehicle design.

Depending on the extent to which the fuel cell is the primary power source, the dynamic response of the complete fuel cell system can be quite important. For example, in the range-extender paradigm, a delay of several seconds in starting the fuel cell may not be significant. In that application, it may be that the fuel cell will be started, run at a constant load for a required period of time and then shut down until needed again. In contrast, if a fuel cell system is a vehicle's primary power source, then the system dynamics are quite important, as power demands can fluctuate quite rapidly during the drive cycle. In that application, time lags or sluggish responses may be unacceptable or even hazardous. The dynamic response of a fuel cell system can

* Corresponding author. Tel.: +1 205 348 2605; fax: +1 205 348 6419.
E-mail address: kwilliams@eng.ua.edu (K.A. Williams).

0378-7753/$ – see front matter © 2006 Elsevier B.V. All rights reserved.
doi:10.1016/j.jpowsour.2006.10.016

therefore be an important part of realizing safe operation of fuel cell vehicles.

Fuel cell dynamics have been studied from a variety of different perspectives. For example, a number of authors have examined the interactions between fuel cells and power conditioning circuits, including Gemmen [1], Fontes et al. [2], Choi et al. [3] and Schenck et al. [4], to name a few. In those works, the authors were generally concerned with obtaining an understanding of how the power conditioning circuits, including DC/AC inverters and boost and DC–DC converters, can affect the ripple current of a fuel cell system. Gemmen [1] provides a definition of ripple current as a deviation of the system current away from the current, which is theoretically obtainable for a given set of reactant flows. He noted that inverter loads can, in some cases, cause ripple that is potentially damaging to fuel cell membranes.

Another approach to studying the interactions between fuel cells and power conditioning was taken by Fontes et al. [2] and Choi et al. [3], who performed experiments to determine the dynamic impedance of a fuel cell systems. Fontes et al. concluded that the charge double layer (CDL) capacitance of the fuel cell was sufficient to filter the high-frequency ripple, but the lower frequency interactions may be of concern. Choi et al. examined the effect of the low-frequency ripple on fuel cell power output and proposed limits on the allowable ripple so as to minimize fuel cell power losses. Those authors also proposed the use of their model to optimize fuel cell/power conditioning unit design in future work.

Fuel cell transient responses have also been studied by a number of authors. Morner and Klein [5] examined the influence of temperature, humidity and air flow rate on the transient performance of a fuel cell stack. Wang and Wang [6] developed a simulation model to study the influence of operating parameters on fuel cell system performance. Those authors included a determination of time constants for both the CDL capacitance effect of the fuel cell, gas transport within the cells and water content of the membrane, with the intent of using the information in future works dealing with the design of power circuits and fuel cell system control.

The response of a fuel cell system subjected to large load variations was studied by Hamelin et al. [7]. The authors reported that the fuel cell system was able to respond to load variations within 0.15 s, although they also noted the presence of large current and voltage transients that may require filtering. Pei et al. [8] described the development of a test stand for testing vehicle-scale fuel cells. The authors reported on the use of the system to test a 50 kW fuel cell and presented results on the fuel cell efficiency. Transient responses were also reported by some of the authors examining fuel cell/power conditioning interactions. Fontes et al. [2] examined the transient responses of a 200 W fuel cell to 20 kHz switching. Schenck et al. [4] studied fuel cell responses for 60 Hz inverter loads and also for step load changes. In working with the step loads, the authors examined not only the large time-scale (integer seconds) responses, but also the response at a fairly small time-scale (tens of micro-seconds). The authors suggested the use of ultra capacitors to reduce the ripple of the output signal.

In examining the literature, it is apparent that there is a growing interest in the dynamic and transient responses of fuel cell systems. A good deal of the research has focused on the development of models so that simulation studies can be performed to determine the appropriate methods for designing fuel cell and power conditioning system interactions. Comparatively fewer works have been found that deal with the transient response of fuel cell systems to arbitrary load changes, although a great deal of simulation work has been carried out in that area. For example, Pukrushpan et al. [9] and Guezennec et al. [10] have developed fuel cell system simulations that are used to study the dynamics and control of fuel cell systems in vehicular applications. A more recent work that has dealt with the dynamic response of fuel cells is the paper by Lemes et al. [11], who discussed the development of a system for performing hardware in the loop simulation with fuel cell system components. The intent of that work is the development of a platform such that individual components can be implemented and optimized as if they were in a complete physical system, even though part of the system is actually implemented in simulation, rather than in physical hardware. Another work that deals with fuel cell dynamics is the report produced by Ottesen [12]. In that work, the author describes basic testing of a Nexa fuel cell system identical to the one described in this paper. The Nexa was loaded using a resistor bank that was switched to one of three resistance values. By monitoring the voltage and current, the author was able to observe the basic behavior of the Nexa system in response to step changes in load. The data collection for that work was done at 10 Hz, however, indicating that the examination of the fuel cell dynamics was limited to frequencies below 5 Hz. In addition, as noted, the load variations were restricted to three distinct levels, while in vehicular applications, a more continuous range of load levels is anticipated. There still seems to be room, therefore, for an experimental work that deals with fuel cell system dynamics across a wide range of operating conditions and an examination of the corresponding implications for using the fuel cell system in vehicular applications.

The goal of the research presented in this work is an examination of the dynamic response of a fuel cell system and its implications for the applicability of a fuel cell powerplant as the primary power source in a vehicle. For the purposes of this work, this method of implementing the fuel cell in a vehicle is termed "load-following," as the fuel cell power plant is required to track a given power load demand. To that end, a series of experiments were performed using a commercially available 1.2 kW fuel cell system equipped with a pulse-width-modulated (PWM) DC–DC converter, specifically, a chopper, to regulate the power dissipated over a resistive load. It is understood that automotive applications will require significantly higher power levels than 1.2 kW. However, the smaller fuel cell system is a good start for understanding fuel cell system dynamics; it is more economical and is readily available for researchers in the field. Also, while it is accepted that it may not be possible to directly scale the results from the smaller system to expected results from an automotive system, it is not unreasonable to expect that the general trends will hold as the system size is

increased. It is important to acknowledge that it is definitely possible to utilize a fuel cell in a load-following mode; in their paper, Winter and Herman [13] describe some characteristics of General Motors' HydroGen3 fuel cell vehicle. The authors made the point that a significant improvement in the HydroGen3, as compared to previous generations of fuel cell vehicles, was the elimination of the "high performance buffer battery" used to provide power during peak demands, through improvement of the fuel cell system's dynamic response. That would seem to imply the utilization of the fuel cell system in a load-following mode, further reinforcing the notion that a thorough knowledge of fuel cell system dynamics is an important topic that deserves attention.

The first set of tests performed with the fuel cell system was an examination of the AC response of the fuel cell. Tests were performed for various DC offset and AC amplitude combinations. For each test, an AC signal superimposed over a fixed DC offset was applied to the PWM input, which then drove the DC–DC converter accordingly. DC offsets from 20% to 80% duty cycle and AC amplitudes from 10% to 40% duty cycle were used to provide a thorough examination of the system response across the bulk of the system's operating range. AC frequencies ranged from 1 to 400 Hz for each test.

The second set of tests consisted of half-cosine increases in the DC–DC converter PWM signal from 10% duty cycle to 90%. The PWM signal was then held at that level for a fixed dwell time before being brought back down to the original 10% duty cycle level.

The intent of those tests was to provide data on the fuel cell system's response to a sudden change in the DC power output, the principle being that, the system's response to AC power fluctuations may or may not correlate well with its ability to deal with sustained load changes in sustained loads.

After evaluating the open-loop behavior of the fuel cell system, a classical proportional–integral (PI) controller was developed to regulate the fuel cell system's power output. The controller was then used to drive the fuel cell system's power output to match half-cosine/dwell transient signals similar to those used in the open-loop tests. The fuel cell system was then exercised with a simulated drive cycle. The PI controller was modified to regulate the power dissipated over the load. The vehicle simulation package Powertrain System Analysis Toolkit (PSAT) was then used to generate a drive cycle history for a conventional vehicle on the Federal Urban Drive Schedule (FUDS). The maximum power required during that drive cycle was approximately 70 kW. The power signal was then scaled down to a maximum of 700 W and used as a reference input to the PI controller.

The experimental setup is described in the next section of this work. The results from the stepped-sine tests are then presented and are followed by a description of the open-loop transient tests. The PI controller development and its application to tracking transient signals are then presented. Finally, the performance of the closed-loop system in tracking the drive schedule is described. Conclusions follow, along with suggestions for future work.

2. Experimental setup

The fuel cell system used in this effort was a Ballard Nexa 1.2 kW fuel cell system. The benefit of choosing that system is that it is a completely integrated fuel cell system that is commercially available and requires minimal effort to setup in a laboratory. Some method of regulating the Nexa output is required, however, in order to use the Nexa for producing practical power. In this case, a DC–DC converter was developed using an insulated gate bipolar transistor (IGBT) and associated gate drivers. Specifically, the IGBT was used to create a chopper circuit, where the IGBT acted as a high-frequency switch between the fuel cell system and the load. By switching the IGBT at a high-frequency and by modulating the percent duty cycle of the device, continuous variations in the power dissipated across the load were realized. It is understood that more sophisticated DC–DC converters may be necessary in actual vehicular applications, the basic PWM-driven chopper was judged to be a good start, due to its simplicity and ease of construction. The specific IGBT used in the chopper circuit was a Powerex model CM400HA-12H. The device is capable of switching up to 400 A and is substantially oversized for the Nexa, which is capable of providing up to almost 50 A of current. As such, some performance loss was anticipated in terms of the chopper efficiency. The issue of sizing power electronics for efficient integration with a fuel cell system will be addressed in a future work. The IGBT was driven using a gate-drive constructed according to the manufacturer's specifications. In turn, the switching signal for the gate drive was generated using a circuit that accepted a 0–10 V analog signal and produced a PWM waveform varying between approximately 2% and 95% duty cycle at approximately 20 kHz. It should be noted that duty cycles below 2% and above 95% were disallowed to prevent the IGBT from operating in the active region indefinitely. Such operation would result in significant power dissipation in the IGBT and would result in damage or destruction of the device.

To dissipate the fuel cell power, a variable load bank was constructed using power resistors and solid-state relays. A schematic of the load-bank is shown in Fig. 1. Through appropriate switching of the relays, the resistance of the load bank could be varied from 1 kΩ down to 0.56 Ω in 1024 steps. As shown in the schematic, the higher-valued resistors were Ohmite resistors rated for 100 W of power dissipation. The lower-valued resistors were Huntington Electric, Inc. Edgewound resistors with 1 kW power dissipation ratings. The original intent was to provide a computer-controlled load bank that could be used independently of the chopper. In the tests reported in this work, however, the load resistance was kept at the minimum level of 0.56 Ω by keeping all of the solid-state relays closed during testing. A 14 Ω rheostat was then added in parallel to the other resistors, so that the load-bank resistance could be further decreased, if necessary. A second 14 Ω rheostat was also included in series with the 1.25 Ω resistor in the load bank, but was kept shorted for the 0.56 Ω tests. If necessary, the second rheostat could be used to increase the overall impedance of the load. A picture of the Nexa, the chopper and the variable load bank is shown in Fig. 2. A more detailed picture of the chopper is shown in Fig. 3.

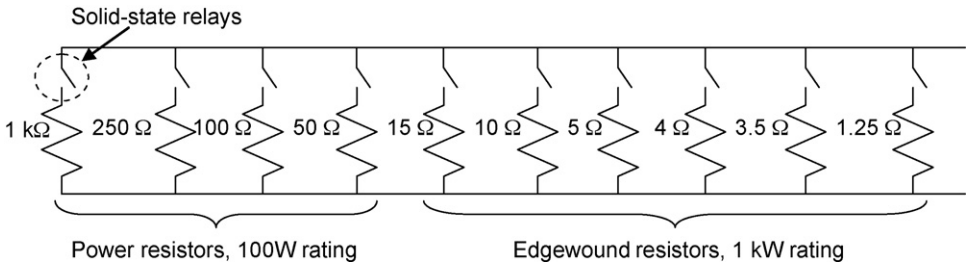

Fig. 1. Schematic of resistive load *i*th solid-state relays.

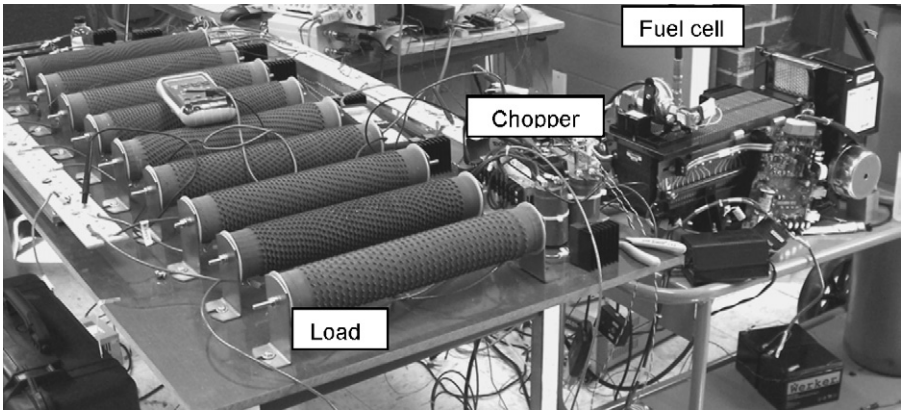

Fig. 2. Experimental setup showing load and fuel cell.

The control and data acquisition tasks were performed using a pair of personal computers running the Mathworks software package XPC Target. That package is used in conjunction with the software Matlab and Simulink. Data acquisition and control software is written in Simulink on a Windows-based "host" PC. The code is then compiled and an executable is sent over a network cable to a "target" PC running a proprietary Mathworks operating system. The executable is then "driven" over the network from the host PC. For the experiments reported in this work, the sampling rate of the target PC was kept at 10 kHz.

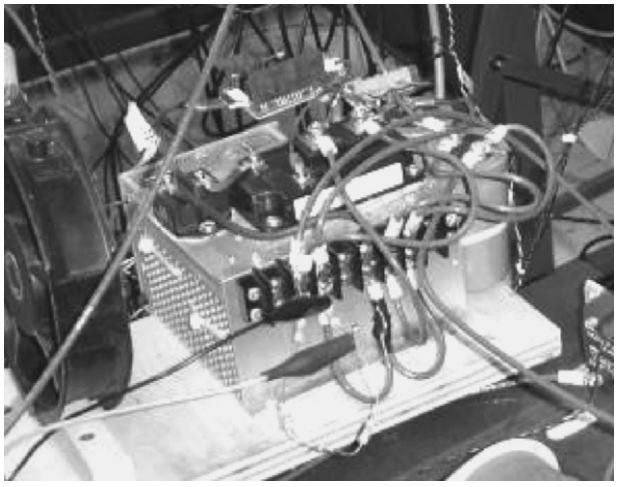

Fig. 3. Close-up of chopper mounted on heat sink.

To determine power produced and absorbed at different points, voltage and current were measured across and through: (a) the Nexa stack, (b) the input to the chopper and (c) the resistive load. The measurement locations are shown in the schematic of Fig. 4, where the stack, chopper, and load voltage and current are labeled V_{st}, i_{st}, V_{chop}, i_{chop}, V_{load} and i_{load}, respectively. Also shown in the figure, the path of the parasitic current, $i_{parasitic}$, which is the current drawn from the stack that is used to power the fuel cell auxiliary systems. All current measurements were made using model LA55-P Hall-effect current sensors produced by Lem. Analog, four-pole, Butterworth, low-pass filters set at 5 kHz were used to filter the analog signals before they were sampled by the target PC. The instantaneous power at each location was then determined as the product of the voltage and current at each point. The chopper switching frequency was approximately 20 kHz and the PWM duty cycle was varied using an analog output from the target PC.

It is important to note that no measurements of the total power produced by the fuel cell were made. According to the Nexa User's Manual [14], when the system is producing the rated load of 1.2 kW, approximately 1.65 kW of heat are produced in the stack, due to the internal impedance of the stack. Future works will examine the overall efficiency of the stack by utilizing hydrogen flow meters during tests. For this work, however, such meters were not available and the only power signals considered are the electrical power coming out of the stack assembly, the power going into the chopper and the power dissipated over the load.

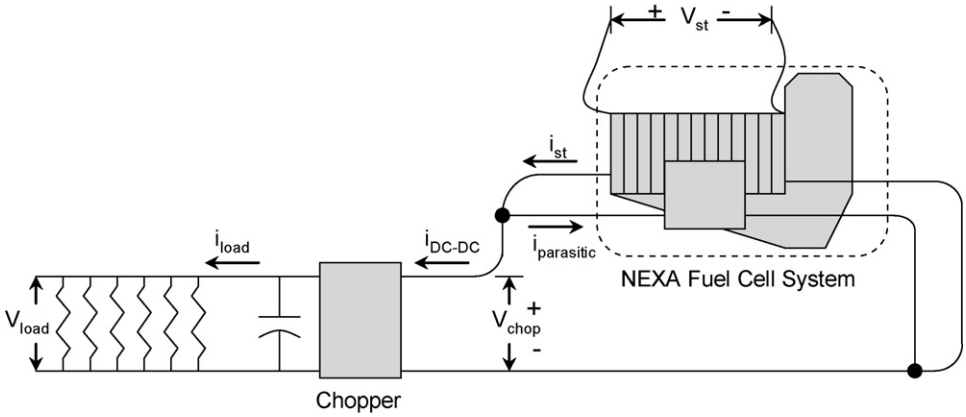

Fig. 4. Testing signal schematic.

3. Open-loop test results

3.1. Preliminary tests: power versus PWM duty cycle

A preliminary test was run to determine the Nexa power output as a function of PWM duty cycle. The PWM input voltage was swept from 0 up to 10 V and then back down again at a rate of 0.1 V s^{-1}. The 0–10 V sweep was intended to correspond to a PWM duty cycle variation from 0% to 100%, or a rate of 1% duty cycle per second. The fuel cell stack electrical power, the power at the chopper input and the power dissipated over the resistive load are shown as functions of the PWM input signal in Fig. 5.

Certain interesting characteristics of the fuel cell system are seen in Fig. 5. First, the chopper input power is always less than the stack power. This is because the Nexa uses some of its power to run the air compressor, cooling blower motor and other parasitic loads. Next, the load power is seen to be substantially less than the other two power levels. This is due to the efficiency of the chopper. The relative electrical efficiencies of the fuel cell system and the chopper during the PWM sweep are plotted in Fig. 6. It should be noted that in the figure, only electrical efficiencies are considered. That is, the chopper/stack efficiency is the ratio of chopper input electrical power to stack electrical power. No consideration is given to the overall system efficiency in terms of fuel used. In examining Fig. 6, it is seen that the fuel cell parasitic loads are most significant at low output power levels. This is attributed to there being a minimum power required to operate the Nexa that is independent of the output power. Beyond the 20% duty cycle, however, the parasitic loads appear to be proportional to the duty cycle, such that the efficiency improves to more than 95% for most of the operating range.

In examining the load/chopper and load/stack efficiencies, it interesting to note that the efficiency is initially very poor, but that it improves to more than 60% at the higher loads. This is attributed to switching losses in the chopper. At low loads, the switching losses of the chopper are large, relative to the amount of power passed to the load. As the power per switch cycle increases, the switching losses are maintained at approximately the same level and the overall chopper efficiency improves.

One other interesting characteristic of the fuel cell system is seen in Fig. 5. There is an apparent hysteresis in the stack electrical power, which is then reflected in the chopper and load powers, as well. The hysteresis is attributed to the stack warming

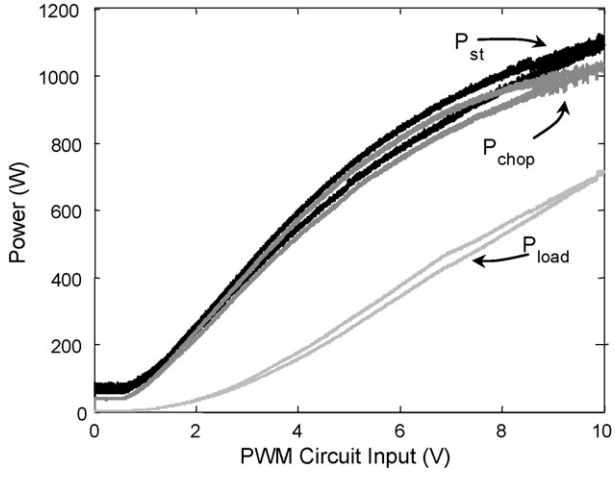

Fig. 5. Experimental fuel cell stack, chopper and load power as a function of the PWM input voltage.

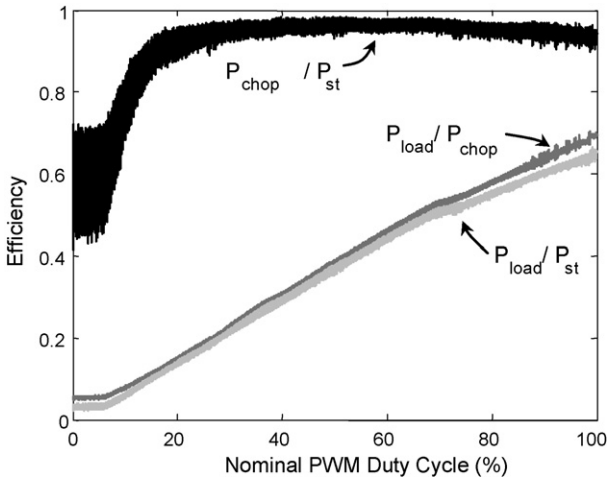

Fig. 6. System electrical efficiencies during PWM sweep.

up during the sweep, such that the stack was able to produce more power at a given load setting. To alleviate such behavior, the system was operated for 5 min at approximately 240 W prior to the ramp test.

Overall, the data presented in Fig. 5 suggests that the fuel cell/chopper combination is capable of providing a DC power output that is a fairly linear function of duty cycle across most of the operating range. The slope of the stack electrical power versus PWM input signal does lose some gain as the input signal is increased, but for perturbations about most operating points, the power versus PWM input signal does appear quite linear. Further, if the power dissipated across the load is considered, the system is very linear for most power levels. Certainly, the non-linearities that are evident in Fig. 5 should not present great difficulties for regulating the power if a feedback controller is used.

Table 1
Stepped-sine PWM input signals

DC offset (V)	AC amplitude (V)	Nominal duty cycle (%)
2	1	20 ± 10
3	1	30 ± 10
3	2	30 ± 20
4	1	40 ± 10
4	2	40 ± 20
4	3	40 ± 30
5	1	50 ± 10
5	2	50 ± 20
5	3	50 ± 30
5	4	50 ± 40
6	1	60 ± 10
6	2	60 ± 20
6	3	60 ± 30
7	1	70 ± 10
7	2	70 ± 20
8	1	80 ± 10

3.2. Stepped-sine tests

As a first step toward examining the dynamic performance of the Nexa system, an offset sinusoidal signal was applied to the PWM input and stepped through frequencies from 1 to 400 Hz. The test was performed for 16 different combinations of DC offsets and AC amplitudes. The complete set of offsets and amplitudes is shown in Table 1, along with the nominal % duty cycles.

Prior to each stepped-sine test, the system was run at the test's DC power level for 6 min. The AC signals were then started at 1 Hz. The frequencies varied in 1 Hz increments out to 10 Hz, then in 2 Hz increments out to 50 Hz, and finally in 5 Hz increments out to 400 Hz. At each step in frequency, the system was run for a specified dwell time. Dwell times were 10, 2 and 1 s, for the 1, 2 and 10 Hz frequency steps, respectively. To process the data from each test, a program was written to calculate the FFT of the data for each step in frequency. In that fashion, the system's frequency response could be obtained as the magnitude of the response at the excitation frequency. In addition, the amplitudes of any harmonics could be used as indicators of non-linear behavior. A plot of the resulting frequency spectra of the stack power is shown in Fig. 7 for the case of a duty cycle with a nominal 50% DC offset and 40% AC amplitude. That specific case was chosen because it utilized the largest AC amplitude of any of the tests and, as such, would be expected to produce the most significant non-linearities in the response. It should be noted that, to make the figure more clear, the spectra plotted in

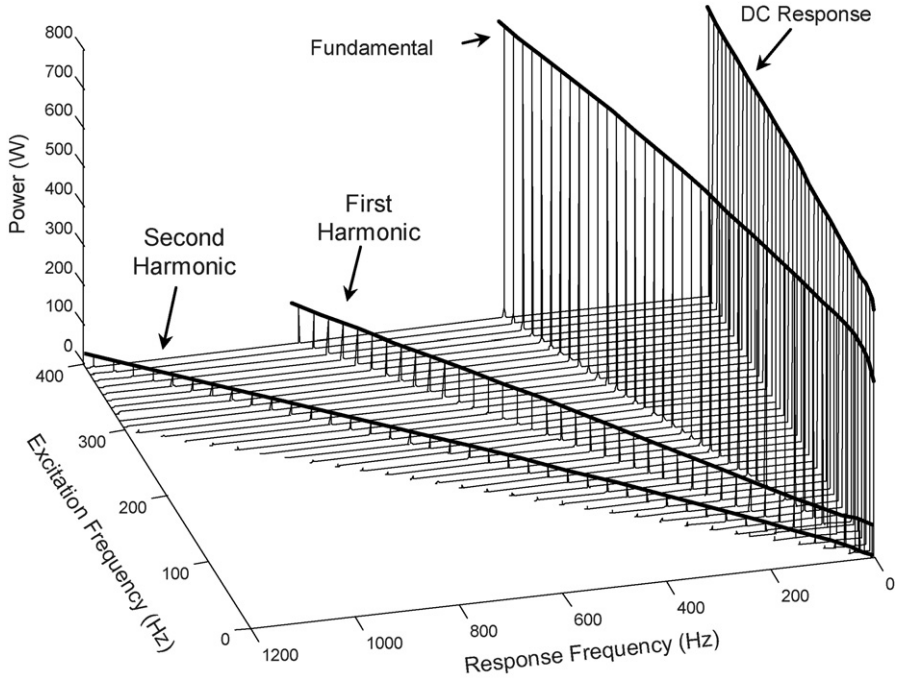

Fig. 7. Frequency spectra of NEXA stack power as function of excitation frequency.

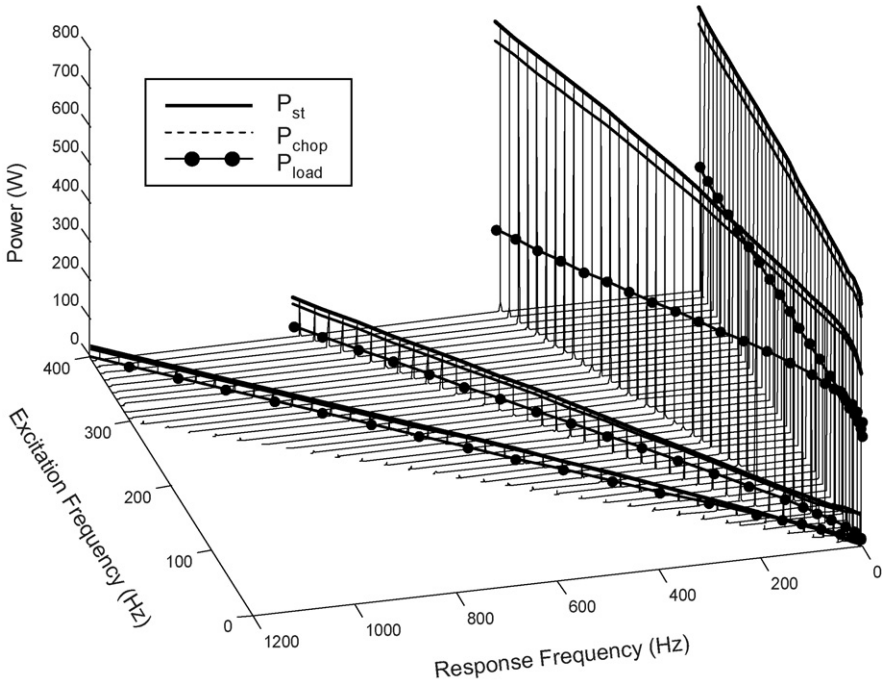

Fig. 8. Frequency spectra for NEXA stack power, chopper input power and power dissipated over the load as function of excitation frequency.

Fig. 7 correspond to frequencies that are integer powers of ten. Inclusion of spectra for all frequencies that were tested would have resulted in a more convoluted plot. To better highlight the data, lines were drawn connecting the peak response amplitudes of the different spectra, as well as the first and second harmonics and the DC amplitudes. The same data is then plotted in Fig. 8, but with the addition of lines indicating the peak amplitudes of the chopper input power and the power dissipated over the load.

In examining the data shown in Figs. 7 and 8, it is apparent that non-linearities are present, as evidenced by the response of the first and second harmonics. However, it is also apparent that the system's response at those harmonics is quite small, in comparison to the response at the fundamental (excitation) frequency. Another interesting characteristic of the plots is that the stack power amplitude increases as the frequency increases. This would seem to correlate well with results presented by Fontes et al. [2] and Choi et al. [3], who both reported a decrease in the internal electrical impedance of fuel cell systems as a function of frequency up to frequencies in the range of 1 kHz. To see that behavior more clearly, the fuel cell stack and chopper power amplitudes at the fundamental frequencies were plotted as a function of excitation frequency in Fig. 9. The corresponding load power responses are shown in Fig. 10. The increasing power amplitudes as a function of frequency are more apparent in Fig. 9. That would seem to be indicative of a decreasing fuel cell impedance as a function of frequency.

To further investigate the variation of the stack electrical impedance with frequency, the electrical impedance of the stack at each frequency was determined by dividing the amplitude of the voltage by the amplitude of the current at each excitation frequency. Resulting impedance plots are shown in Fig. 11 for the PWM DC offset of 50% and AC amplitudes of 10%, 20%, 30% and 40%. The plots are similar to the plots shown in the works by Fontes et al [2] and Choi et al. [3]. As seen in Fig. 11, the stack impedance is not a significant function of AC amplitude. To investigate the effect of the PWM duty cycle DC offset, plots of the stack impedances are shown in Fig. 12 for PWM duty cycle AC amplitudes of 10% and DC offsets of 20%, 30%, 40%, 50%, 60%, 70% and 80%. As seen in Fig. 12, the DC offset has a more significant effect on the stack electrical impedance than does the AC amplitude (the effect of which is shown in Fig. 11 for the case of the DC offset of 50% duty cycle). This is attributed to the shape of the typical voltage versus current plot for a fuel cell stack, also known as a polarization curve. Exam-

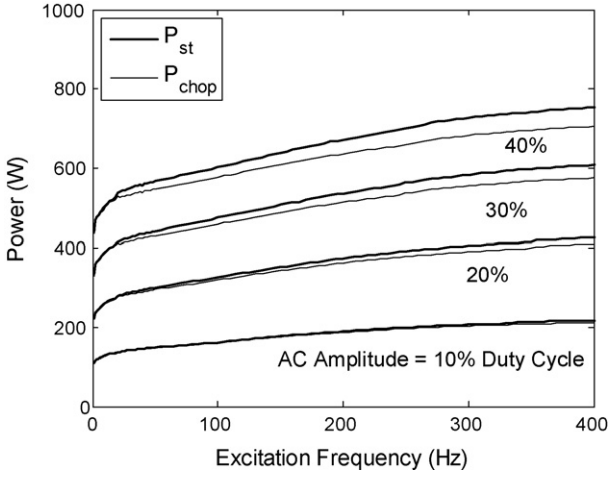

Fig. 9. Stack and chopper AC power as a function of excitation frequency for 50% DC offset in PWM duty cycle and various AC amplitudes for 0.56 Ω load impedance.

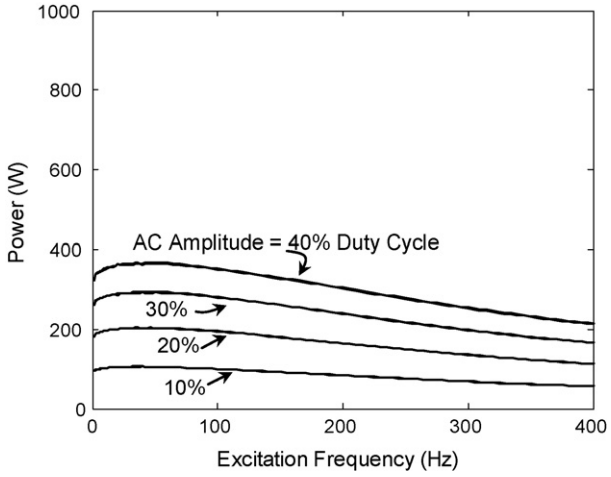

Fig. 10. Load AC power as a function of excitation frequency for 50% DC offset in PWM duty cycle and various AC amplitudes for 0.56 Ω load impedance.

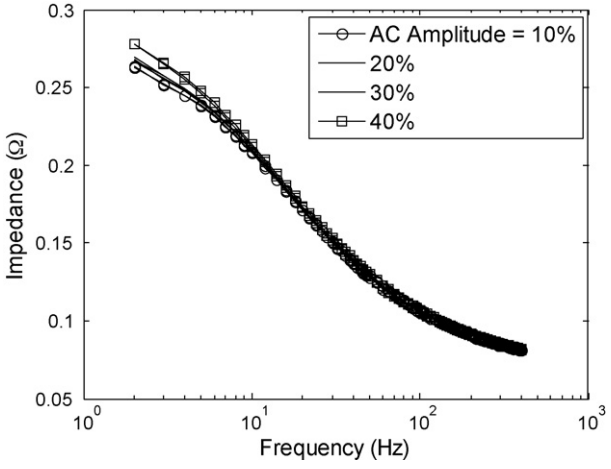

Fig. 11. Experimental stack impedance as a function of PWM duty cycle AC amplitudes at a 50% DC offset.

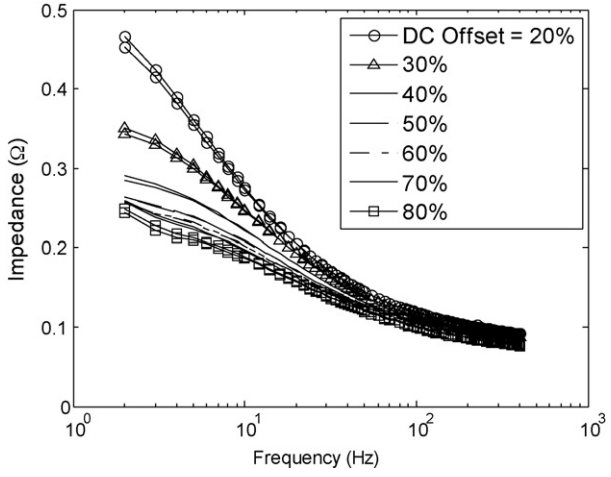

Fig. 12. Experimental stack impedance as a function of PWM duty cycle DC offset for 10% AC amplitudes.

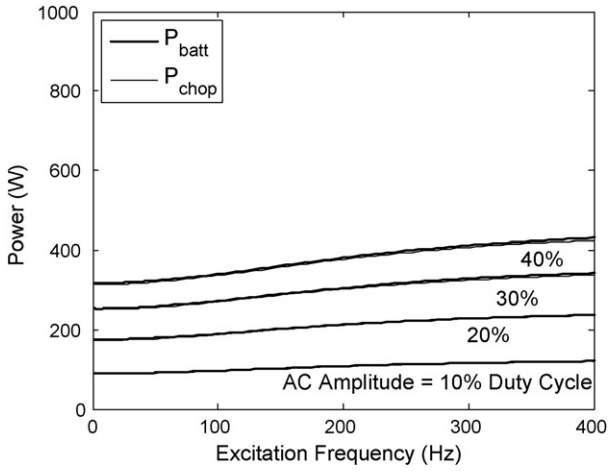

Fig. 13. Battery and chopper AC power as a function of excitation frequency for 50% DC offset in PWM duty cycle and various AC amplitudes for 0.56 Ω load impedance.

ples of such curves are shown in a number of sources, including the text by Larminie and Dicks [15]. For small duty cycles, the stack is operating in a region of the polarization curve where small variations in current result in large voltage changes.

However, with increasing current densities, or equivalently, increasing percent duty cycle, the voltage versus current slope flattens out, such that large current variations can be obtained with very small voltage changes. As the variation of voltage over the variation in current is the impedance of the stack, operating at higher DC offsets of percent duty cycle thus results in a lower stack impedance.

As a check on the results of the fuel cell stepped-sine tests, similar stepped-sine tests were performed after replacing the fuel cell with two pairs of Optima® YellowTop 12 V batteries. Each pair of batteries were wired in parallel and the two pairs were then wired in series to produce an approximately 25 V power supply. The stepped-sine tests were then repeated for the case of the 50% DC offset and AC amplitudes of 10%, 20%, 30% and 40%. The resulting battery and chopper power amplitudes as a function of frequency are shown in Fig. 13 and the corresponding amplitudes of the power dissipated over the load are shown in Fig. 14. In Fig. 13, the chopper amplitudes are only slightly smaller than the battery power amplitudes, in contrast to the corresponding results for the fuel cell tests. The reason for this is that a significant amount of the fuel cell stack electrical power is diverted and used to run the balance of plant. In contrast, in the case of the battery tests, the only difference between the battery power and the chopper power is the small amount of power lost over the blocking diode. It is immediately obvious that the battery power amplitudes shown in Figs. 13 and 14 are significantly less than the corresponding fuel cell and load power amplitudes shown in Figs. 9 and 10. The main reason for this is that the combined battery voltage was approximately 25 V, both open-circuit and under load. The fuel cell open-circuit voltage was approximately 44 V, but dropped down to range from approximately 33.5 V the beginning of the stepped-sine test to 32.2 V at the end of the test, or an approximate average voltage of 32.85 V. To compare the fuel cell and battery responses, the

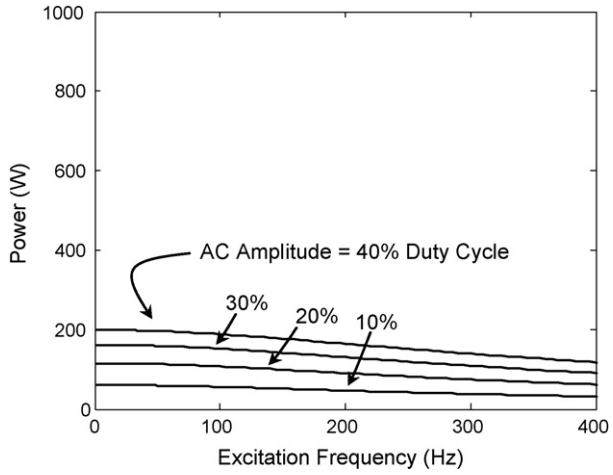

Fig. 14. Load AC power as a function of excitation frequency for 50% DC offset in PWM duty cycle and various AC amplitudes for 0.56 Ω load impedance.

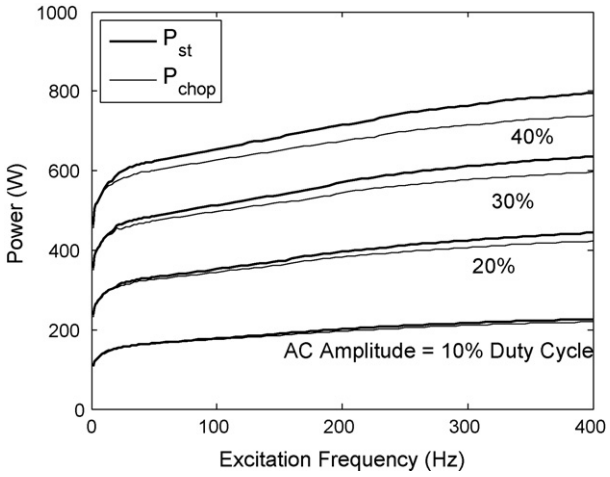

Fig. 16. Stack and chopper AC power as a function of excitation frequency for 50% DC offset in PWM duty cycle and various AC amplitudes for 0.45 Ω load impedance.

battery power levels were scaled by a factor of 1.73 (determined as the square of the ratio of 32.85 divided by 25 V). The fuel cell stack power amplitudes and the scaled battery power amplitudes are then plotted in Fig. 15. As seen in the figure, for frequencies above approximately 50 Hz, the batteries results are quite similar to the fuel cell results. As such, the fuel cell dynamics seem to be more significant at lower frequencies than at higher frequencies.

With regards to the apparent increase in the power produced by both the fuel cell system and the batteries with increasing frequency, it should not be interpreted to mean that the output power can be increased by demanding a higher frequency load power swing. In actuality, due to the sinusoidal variation of the PWM, the chopper is operating not only in the buck mode, but in the inverter mode as well. Thus, the output capacitor, which is used to reduce ripple on the DC component of the output voltage is in fact subjected to an AC voltage at the power swing frequency as well. The capacitive impedance is inversely proportional to the frequency, and thus, more current is delivered to the capacitor. That power is not, however, passed on to the load, as is apparent

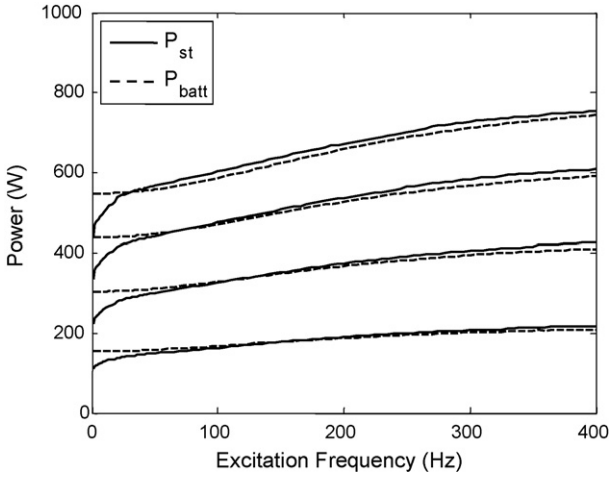

Fig. 15. Stack and scaled battery AC power as a function of excitation frequency for 50% DC offset in PWM duty cycle and various AC amplitudes for 0.56 Ω load impedance.

in examining Figs. 10 and 14. In fact, the power–frequency curve is actually a plot of the magnitude of the instantaneous power amplitude and should not be construed as active or real power. The steady-state concepts of real and reactive power are not represented here.

Overall, the behavior shown in Figs. 7–15 highlights an important issue in the design of fuel cell power systems: the need for careful consideration of the fuel cell and load interactions. As noted previously, this is a theme that is echoed in other articles in this area. In the work by Benziger et al. [16], the authors make the point that impedance matching is a critical issue in determining efficient operating points for a fuel cell system. In that work, the authors present results showing how the power delivered from the fuel cell to the load depends on the load impedance. To examine the effect of driving different load impedances on the power produced by the fuel cell and delivered to the load, the stepped-sine tests were repeated with load impedances of 0.45 and 0.75 Ω. Those two load impedances were obtained by varying the settings on the rheostats added to the original load bank. These additional tests were run for the 50% DC offset and 10%, 20%, 30% and 40% AC PWM amplitudes. The resulting electrical power produced by the fuel cell and delivered to the chopper is shown in Figs. 16 and 17 for the cases of the 0.45 and 0.75 Ω load impedances, respectively. The corresponding traces showing the power dissipated over the loads are shown in Figs. 18 and 19, respectively. In examining those figures, it is possible to discern that, as the impedance of the load goes down, the power produced by the fuel cell increases. For example, at 400 Hz, the 0.45, 0.56 and 0.75 Ω loads result in AC power amplitudes of approximately 800, 750 and 700 W, respectively. The corresponding amplitudes of the power dissipated over the load are approximately 210, 250 and 190 W, respectively. As such, the 0.56 Ω load appears to result in the greatest ratio of electrical power produced by the stack to electrical power dissipated over the load. The result is not surprising, as the rated power of the Nexa is 1200 W and is listed as being realized at a stack output of 26 V and 46 A.

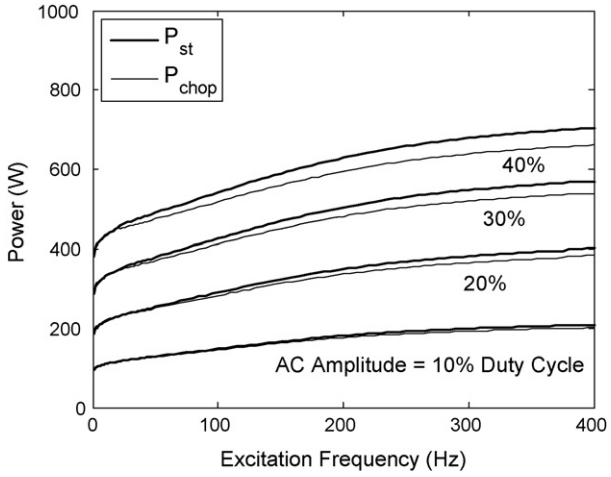

Fig. 17. Stack and chopper AC power as a function of excitation frequency for 50% DC offset in PWM duty cycle and various AC amplitudes for 0.75 Ω load impedance.

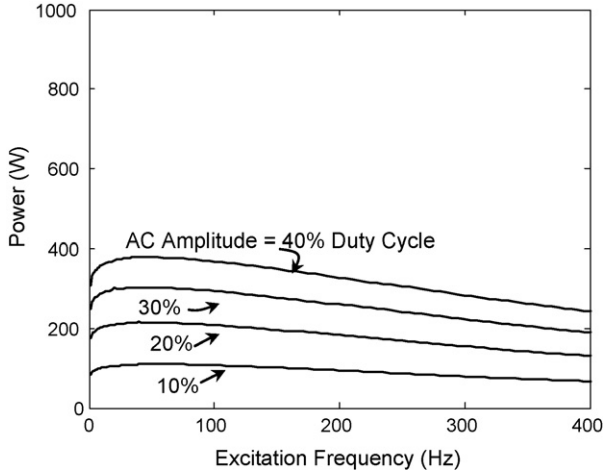

Fig. 18. Load AC power as a function of excitation frequency for 50% DC offset in PWM duty cycle and various AC amplitudes for 0.45 Ω load impedance.

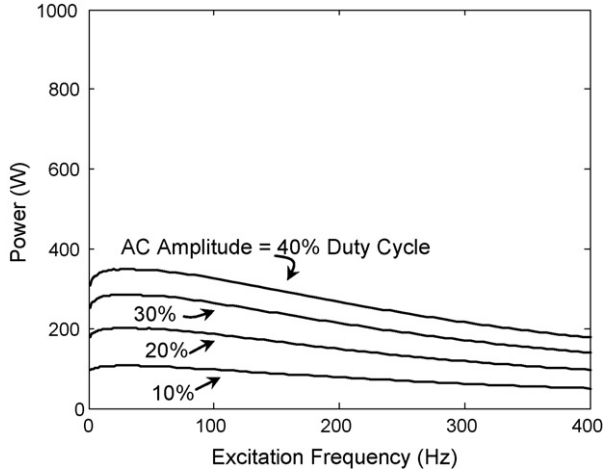

Fig. 19. Load AC power as a function of excitation frequency for 50% DC offset in PWM duty cycle and various AC amplitudes for 0.75 Ω load impedance.

The voltage and current correspond to a resistance of approximately 0.565 Ω. This conclusion was also supported by an examination of the DC power dissipated over the load for each resistance level. For the 0.45, 0.56 and 0.75 Ω loads, the DC power dissipated over the stack at the end of the stepped-sine tests was approximately 267, 290 and 282 W, respectively (30 s of dwell at the DC % duty cycle with no AC variations were provided at the end of each test). Again, as noted previously, and as presented in the paper by Benziger et al. [16], effective utilization of a fuel cell system requires careful consideration of interactions between the fuel cell system and the load.

In considering the results of the AC testing, three particular points can be made:

- System efficiency is highly dependent on load; with the specific configuration used in this work, switching losses severely impact efficiency at low loads.
- There are strong relations between stack impedance and both AC frequency and DC offset. Those may have important implications for power conditioning circuit design.
- Overall, the system does respond quite well to AC load variations and there is no apparent "roll-off" in the frequency response that will negatively impact load following in the frequency range of interest.

However, while it is true that the AC response of the fuel cell system is quite good, that performance may not directly translate to good transient performance. This is somewhat in contrast to conventional wisdom in the controls community, which regards bandwidth and transient response as comparable metrics. For example, in the case of a servo-system, it is reasonable to expect that high-bandwidth actuators are required to attain fast transient responses. In the case of the fuel cell, however, it is possible to pull short bursts of power from the stack, due to the CDL capacitance. In addition, there is capacitance in the form of the stack volume, which holds a certain amount of reactants available for immediate use. In the case of a step in power demand, it may therefore be possible to attain high power levels for short duration. However, as the CDL capacitance is drained of charge and as the reactants immediately available in the stack are used up, the partial pressures of the reactants in the stack will decrease and the stack voltage will drop. The power drop will persist until the reactant flow mechanisms have had the chance to increase reactant flows to support the new power level. This behavior is noted in other works, including the paper by Schenck et al. [4]. The transient behavior is therefore not completely defined by examining the AC response only. To that end, a different approach to examining the transient performance of the fuel cell system is presented in the next section of this work.

3.3. Transient response tests

A common waveform used to evaluate transient responses is the step function. A great deal of information becomes available when applying such an input to a system. For example, by examining a system's step response it is possible to determine if the system is under- or over-damped, if the system is minimum or

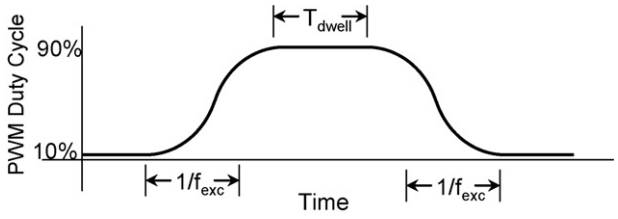

Fig. 20. Waveform used for open-loop transient tests.

non-minimum phase, and, more generally, if the system is "fast" or sluggish. Fell cell system step responses have been examined by other authors including Schenck et al. [4]. In this work, a somewhat modified approach is taken. Rather than using step responses, the input to the PWM is a modified cosine. Specifically, the input has the shape

$$u(t) = \mathrm{DC}_{\mathrm{offset}} + \frac{1 - \cos(2\pi f t)}{2}, \quad 0 \le (2\pi f t) < \pi. \tag{1}$$

In Eq. (1), f is the frequency of the signal for the duration $0 \le t < (1/2f)$. At the time $t = (1/2f)$, $u(t)$ is held constant for a finite dwell time, at which time the signal becomes the reverse of Eq. (1) and smoothly returns to the DC offset. A plot of $u(t)$ is shown in Fig. 20. The "half-cosine" curve was chosen for use in the transient analyses because it both a transient and a quasi-AC signal. Unlike a step function, which theoretically excites a system with all frequencies, the half-cosine curve is band-limited. At the same time, as the frequency in Eq. (1) is increased, the signal approaches a step function in frequency content.

The half-cosine tests were implemented using the same experimental setup as for the AC tests. Frequencies from 0.1 Hz out to 1 kHz were used, each for dwell times of 0 and 5 s. With 0 s dwell times, the signals were essentially inverted cosine pulses at specific frequencies. The fuel cell stack power in response to pulses from 50 Hz to 1 kHz is shown in Fig. 21. As seen in the figure, as the pulse frequency increases, the peak power output from the fuel cell increases. At 1 kHz, the peak power level was more than 2.4 kW, essentially double the rated power output of the NEXA system. Additional responses are shown in Fig. 22

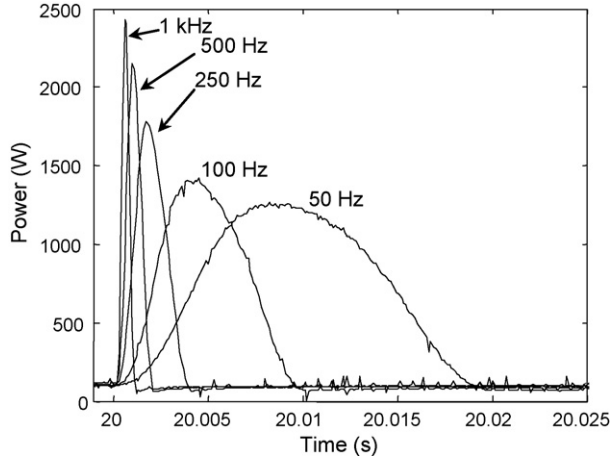

Fig. 21. Pulse responses from 50 Hz to 1 kHz.

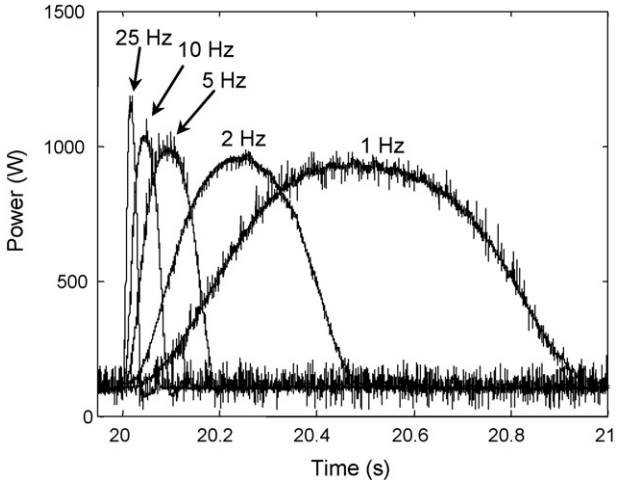

Fig. 22. Unfiltered low-frequency pulse responses.

for frequencies from 1 to 25 Hz. As seen in the figure, there is a considerable amount of high-frequency noise that appears on the signals.

To alleviate that noise, the data was software-filtered with an approximately 160 Hz, first-order, low-pass filter (1 ms time-constant). The filter had a negligible effect on the magnitude and phase of the response, as can be seen by comparing the plots in Figs. 22 and 23.

The second set of pulse tests were performed using a five second dwell at the nominal PWM duty cycle of 90%. A close-up of the unfiltered results for the higher frequency data is shown in Fig. 24. Longer duration plots of similar data after being filtered are shown in Fig. 25. As seen in Fig. 24, the system's response to the transient signals is very similar to its response to the simple pulse signals. Instead of returning to the low power level, however, the responses begin to converge to a higher power level. In Fig. 25, there is an apparent dip in the power during the first 0.5 s of each response. This is attributed to the time needed for the compressor to spin up to increase the air flow to the cathode side of the stack. However, as the compressor spins up, the system responds quite well and appears to reach

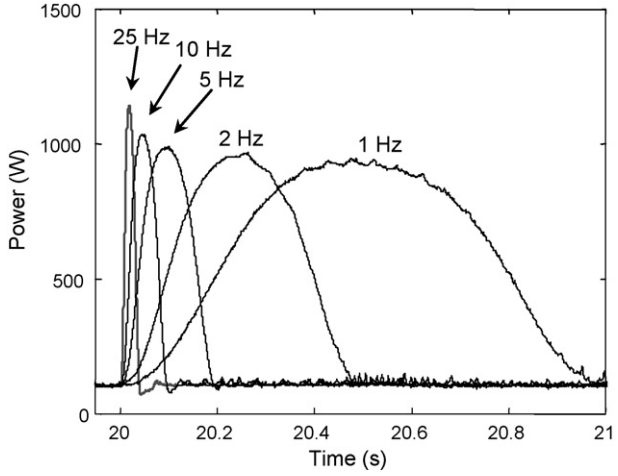

Fig. 23. Filtered low-frequency pulse responses.

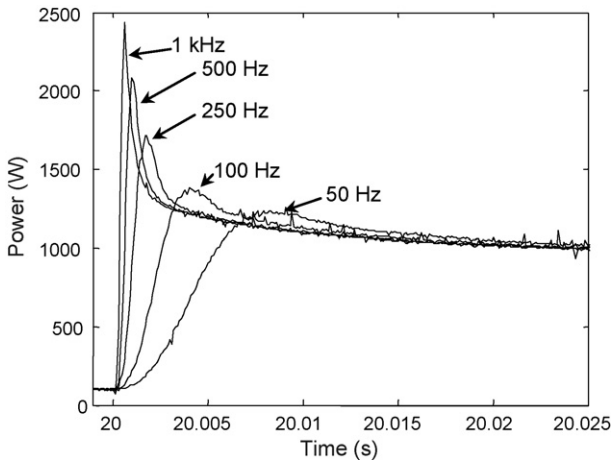

Fig. 24. Close-up of fuel cell power responses to half-cosine inputs with 5 s dwell.

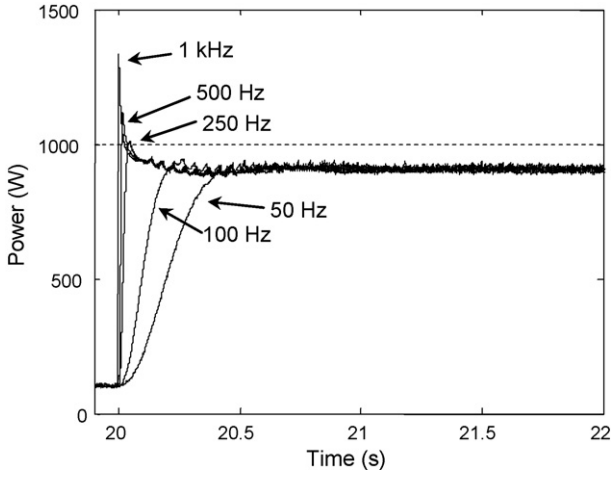

Fig. 25. Plots of fuel cell power responses to half-cosine inputs with 5 s dwells.

the final power level within 1 s. It should be noted that additional increases in power were seen for the longer dwell times. Those increases were relatively slow, however, and are attributed to heating of the fuel cell stack during the tests.

The results of the half-cosine tests show that the transient response of the system is quite good and can respond quite rapidly to sudden load changes. What is quite interesting is the brief surge to high power outputs that occurs with the higher frequency pulses. As seen in Figs. 21 and 24, the power reaches 2.5 kW for a duration on the order of 1 ms. Such surges should not present any problems for the oversized chopper used in this work. However, it is reasonable to speculate as to whether or not a smaller chopper could safely deal with such signals. To deal with that issue, either feedback control or some form of rate-limiting would seem to be appropriate. To that end, the next section of this work presents the results of a feedback controller applied to control the power output of the stack. The controller is then used to control the power absorbed by the load. Finally, the controller is used to regulate the stack and load outputs (in separate tests) during a specific drive cycle.

4. Closed-loop testing

To realize feedback control of the fuel cell power output, the code used for the open-loop testing described in the previous sections was modified. The analog voltage applied to the PWM circuit on the chopper was then produced based on a standard proportional–integral (PI) controller, together with a feed-forward control signal based on the reference power. The PI controller used the difference between a reference power value and a measured power as an error signal. The schematic showing the structure of the PI controller is seen in Fig. 26. Tests were first performed using the stack power as the measured signal, with the goal of making that signal match a reference power in the form of a half-cosine pulse with and without a dwell. The code was then modified so that the load power could track an arbitrary reference signal. For those tests, the reference signal was the scaled power output from a conventional automotive internal combustion engine in a vehicle performing the Federal Urban Drive Schedule.

4.1. Stack power tracking tests

For the first closed-loop tests, a half-cosine signal was generated that was similar to the signal described in Eq. (1). To act as a reference for the stack output, the signal was scaled such that it went from 80 W to a maximum of 720 W. The frequencies used to generate the signals varied from 0.5 to 50 Hz. The 50 Hz upper limit was chosen, as it was judged to be more than sufficient for use in vehicular applications. In addition, because of the significant noise in the system, a fourth-order 1 kHz Butterworth low-pass filter was used to filter the stack voltage and current signals before they were converted to the measured power signal.

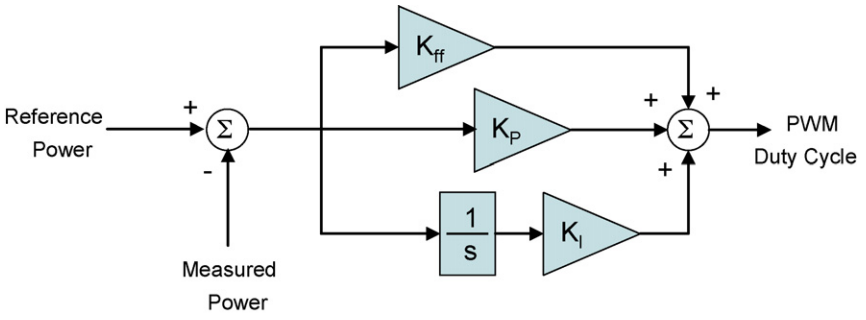

Fig. 26. PI/feed-forward controller schematic.

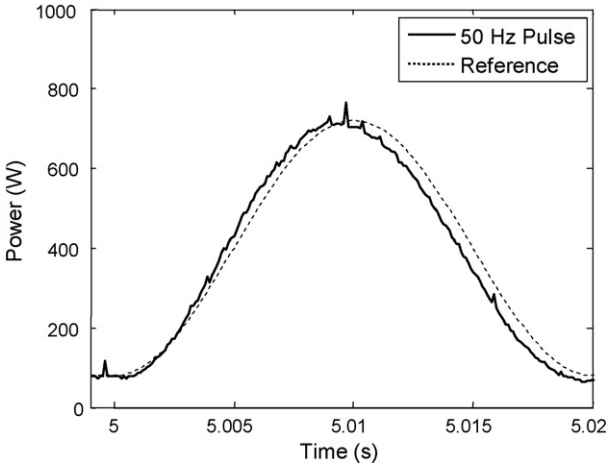

Fig. 27. Nexa stack power output tracking of 50 Hz pulse.

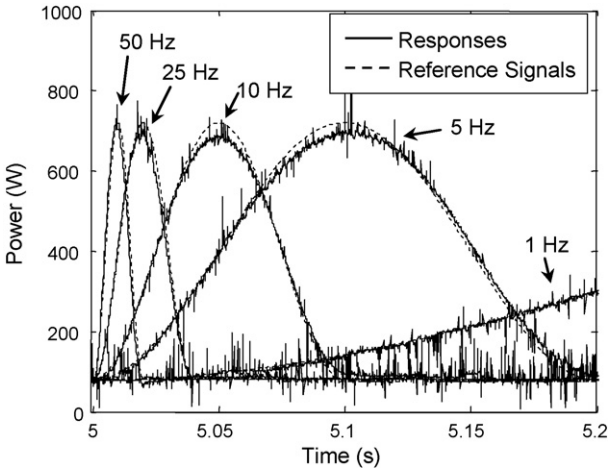

Fig. 28. Nexa stack power output tracking different pulse references.

Also, the control signal generated by the PI controller was filtered by a 1.6 kHz first-order low-pass filter before being applied to the PWM circuit input. The Butterworth filters and the first-order filter added approximately 7.5° and 1.8° of phase lag to the signals at 50 Hz, respectively and, as such, were considered to be negligible for signals with frequency content at and below 50 Hz.

The Nexa stack power in response to a 50 Hz pulse is shown in Fig. 27. In the figure, the reference signal is shown as a dotted black trace. It is interesting to note that the measured power actually leads the reference signal for much of the trace. This is due to the feed-forward element in the controller. The feed-forward is essentially performing open-loop control of the signal and is applying 5 mV of analog voltage to the PWM input of the chopper for every 1 W of reference power. For example, for 100 W of desired power, the feed-forward controller would send a 0.5 V signal to the PWM input, which would nominally correspond to a 5% duty cycle. By taking that approach, the feed-forward signal acts to bring the system output to within the rough vicinity of the desired power and the PI controller is used to more finely tune the power output around that reference value. The 50 Hz pulse trace and the corresponding reference are also shown in Fig. 28, along with pulses at 25, 10, 5 and 1 Hz and their respective reference signals. Finally, the stack power output in response to 1 and 0.5 Hz reference signals is shown in Fig. 29. At first glance, it might appear that there is more noise on the signals shown in Fig. 29 than on those in Fig. 28. This is simply a visual artifact due to the fact that the time scale is compressed in Fig. 29. This is demonstrated by examining the 5 and 1 Hz traces, which appear to have comparable noise levels in Fig. 28. In Fig. 29, however, the duplicate 1 Hz data appears to be significantly noisier.

The next step in the testing was to repeat the closed-loop tests, but for the addition of a dwell time at the peak power output. The Nexa stack power responses to the 50, 25 and 10 Hz half-cosine reference signals with 5 s dwells are shown in Fig. 30. Similar responses to the 5, 1 and 0.5 Hz reference signals are shown in Fig. 31. As with the pulse signals, as the frequency of the reference signal decreases, the noise becomes more apparent. In

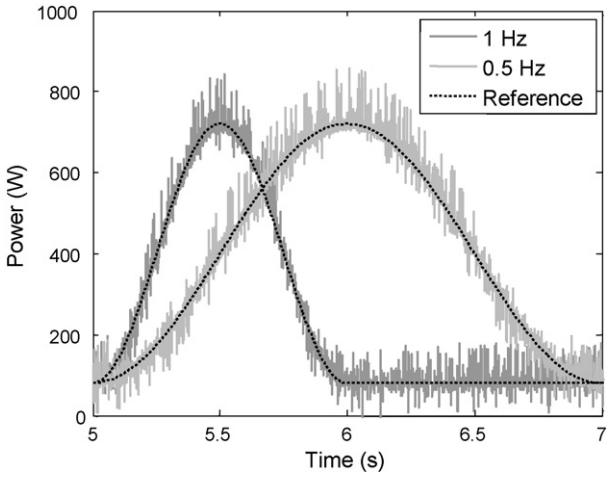

Fig. 29. Nexa stack power pulse responses for 1 and 0.5 Hz references.

Fig. 30, the classical "dip" after the initial increase in power is seen. This is attributed as much to the limitations of the PI controller as to the sudden consumption of reactants within the stack. That is, further increases in the PI gains significantly amplified

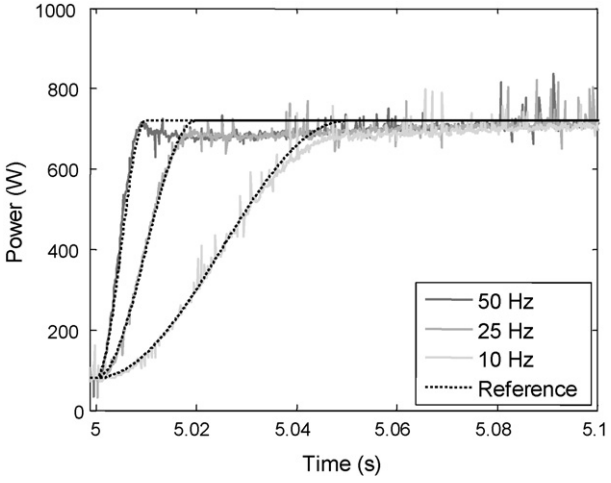

Fig. 30. Nexa stack power in response to 50, 25 and 10 Hz half-cosine references with dwells at peak output.

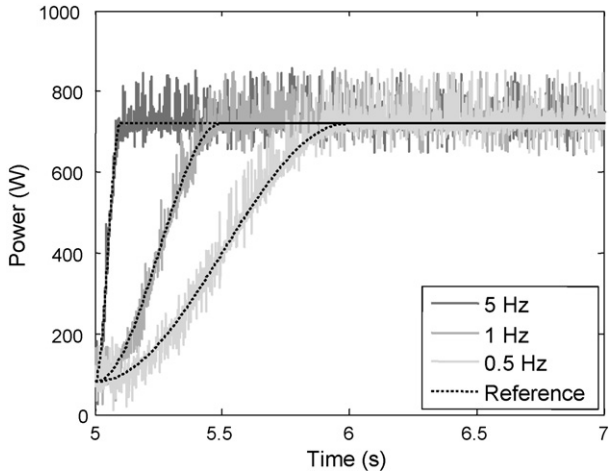

Fig. 31. Nexa stack power in response to 5, 1 and 0.1 Hz half-cosine references with dwells at peak output.

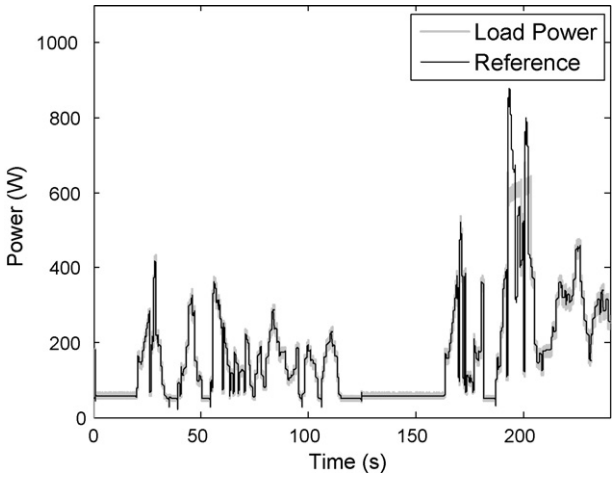

Fig. 32. First 240 s of load power in response to drive cycle power reference signal.

the noise, such that the response began exhibited severe "ringing." As such, the PI gains were kept low and the undershoot in the tracking was accepted. As seen in Fig. 30, however, the integral term very quickly brings the stack power output to be very close to the reference value within 0.1 s. Overall, the responses show that the system can respond quite quickly, attaining within 10% of the final value within 10 ms.

4.2. Drive cycle power tracking

In examining the transient responses, it is apparent that the fuel cell system is quite capable of producing power outputs with closed-loop bandwidths out to 50 Hz and beyond. That would seem to be more than sufficient to enable the fuel cell to be used as a primary power source in a vehicular application. To validate that conclusion, a vehicular drive cycle was generated using the Powertrain System and Analysis Toolkit (PSAT) produced by Argonne National Laboratories. PSAT is a "front-end" that integrates with Matlab and Simulink and enables users to construct vehicle simulation models using a variety of available components, including, among others, internal combustion engines, batteries and fuel cells. Once models have been built, they may be exercised using various available drive cycles. For this work, a conventional 70 kW gasoline-fueled automobile was exercised over the Federal Urban Drive Schedule. The resulting engine power output history varied from a nominal of approximately 0 W out to almost 70 kW. The first 480 s (out of a total of 1372 s) was then scaled down to a power history that varied between 50 and 878 W. The signal was then used as the reference signal for the PI controller that was then used to "drive" the fuel cell system such that the reference power was dissipated across the resistive load bank of approximately 0.6 Ω.

The exact range of the reference power signal was determined by first dividing the 700 W to 70 kW PSAT cycle by a factor of 50 to obtain a reasonable range of powers for the fuel cell stack. The signal was then multiplied by 0.6 to reflect the approximately 60% efficiency of the PWM circuit, resulting in a signal that varied from effectively 0 to 828 W. As noted previously, however, with the specific PWM circuit that was used, there was always some non-zero percent duty cycle applied to the load, due to offset errors in the drive circuit. As such, to avoid integrator wind-up in the controller, the power signal was modified by the addition of 50 W across the entire time history, resulting in the 50–878 W reference control signal. The first 240 s of the resulting load power are shown in Fig. 32, along with the filtered load power (filtered with a 1 kHz, four-pole Butterworth filter) and the reference signal. The same data for the time interval from 240 to 480 s are shown in Fig. 33. To better demonstrate the results, the results from 175 to 225 s and from 230 to 235 s are shown in Figs. 34 and 35.

In Fig. 34, there are a number of important elements of the response that should be considered. First, the controller is unable to drive the system to attain the higher power levels. This is because the efficiency of the chopper significantly reduces the amount of fuel cell power output that can be applied to the load. That is, while the fuel cell system is rated at 1.2 kW of electrical power output, using this particular chopper, the most power that will be absorbed by the load will be on the order of 700 W.

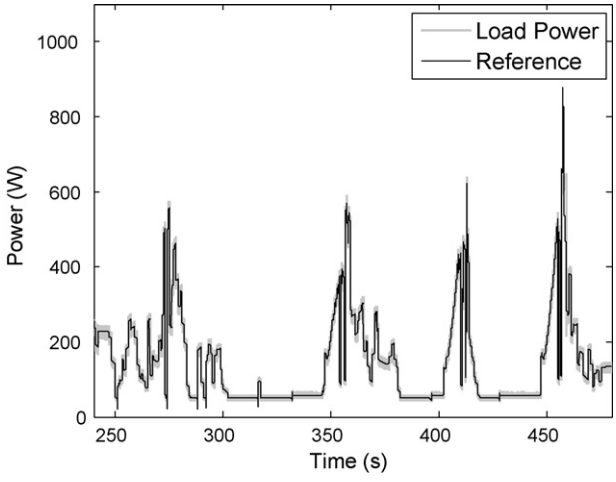

Fig. 33. Second 240 s of load power in response to drive cycle power reference signal.

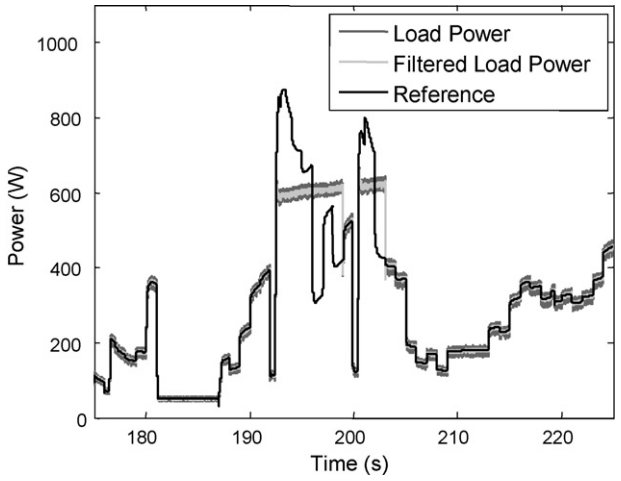

Fig. 34. Load power in response to drive cycle power reference signal, 175–225 s timeframe.

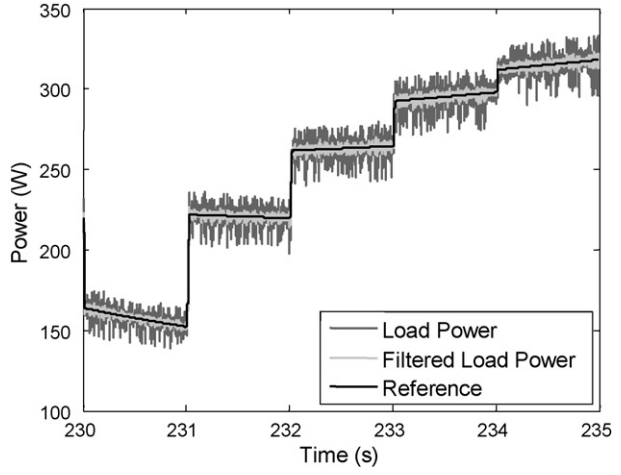

Fig. 35. Load power in response to drive cycle power reference signal, 230–235 s timeframe.

As such, the control signal saturates, the integral term in the controller winds up and the controller then overdrives the system after the reference power drops. The problem of saturating actuators is well-known in the controls community and various forms of anti-windup algorithms will be considered in future works. The point is, however, that the efficiency of the power conditioning circuits is a non-trivial issue that must be dealt with. The other interesting point in the figure is that there is an apparent increase in the fuel cell power output, even after the control signal has saturated. The behavior indicates that the stack is heating with the saturated power output and the available power is therefore increasing with the higher temperature operation. The temperature-dependence of the system performance is thus immediately apparent in those results. Overall, the fuel cell system performance is quite good during the drive cycle. For most of the test, the system was quite capable of responding to transient load variations. This is seen in Fig. 35, where the power output of the system is seen in response to a series of step changes in the reference signal. As shown in the figure, the closed-loop system is able to track the changing reference quite well.

5. Conclusions

This paper has presented the results of an experimental study of the dynamic response of a fuel cell system. The open-loop AC response of the system was evaluated using stepped-sine tests from 1 out to 400 Hz. Transient responses were then performed using half-cosine transitions from 10% to 90% duty cycle, followed by dwells at the 90% duty cycle. The AC and transient results showed that the open-loop bandwidth of the system is quite high. Closed-loop transient responses were then evaluated with the fuel cell power regulated by a PI controller. The controller was then modified to regulate the load power in response to a simulated and scaled vehicle power reference signal. The results indicate that it is feasible to use a fuel cell system in a load-following mode.

Future work will examine the further implications of load-following and its impact on overall system fuel efficiency.

Acknowledgement

Portions of the work presented in this paper were supported by the Center for Advanced Vehicle Technologies at The University of Alabama, which received partial funding from the United States Department of Transportation National Highway Traffic and Safety Administration under grant number DTNH22-04-H-01411.

References

[1] R.S. Gemmen, J. Fluids Eng. 125 (3) (2003) 576–585.
[2] G. Fontes, C. Turpin, R. Saisset, T. Meynard, S. Astier, 2004 IEEE 35th Annual Power Electronics Specialists Conference, PESC04, vol. 6, 2004, pp. 4729–4735.
[3] W. Choi, P.N. Enjetic, J.W. Howze, 19th Annual IEEE Applied Power Electronics Conference and Exposition—APEC 2004, vol. 1, 2004, pp. 385–390.
[4] M.E. Schenck, J.-S. Lai, K. Stanton, Annual IEEE Applied Power Electronics Conference and Exposition, vol. 1, no. 1, 2005, pp. 114–120.
[5] S.O. Morner, S.A. Klein, J. Solar Energy Eng. 123 (3) (2001) 225–231.
[6] Y. Wang, C.-Y. Wang, Electrochim. Acta 50 (6) (2005) 1307–1315.
[7] J. Hamelin, K. Agbossou, A. Laperriere, F. Laurencelle, T.K. Bose, Int. J. Hydrogen Energy 26 (6) (2001) 625–629.
[8] P. Pei, M. Ouyang, Q. Lu, H. Huang, X. Li, Int. J. Hydrogen Energy 29 (10) (2004) 1001–1007.
[9] J.T. Pukrushpan, A.G. Stefanopoulou, H. Peng, Proceedings of the 2002 American Control Conference, vol. 4, 2002, pp. 3117–3122.
[10] Y. Guezennec, T.-Y. Choi, G. Paganelli, G. Rizzoni, Proceedings of the 2003 American Control Conference, vol. 3, 2003, pp. 2055–2061.
[11] Z. Lemes, A. Vath, T. Hartkopf, H. Mancher, J. Power Sources 154 (2) (2006) 386–393.
[12] H. Ottesen, Report for Rochester Public Utilities, Rochester, Minnesota, 2004.
[13] U. Winter, M. Herrmann, Fuel Cells 3 (3) (2003) 141–145.
[14] Nexa™ Power Module User's Manual, Ballard Power Systems, Inc.
[15] J. Larminie, A. Dicks, Fuel Cell Systems Explained, second ed., John Wiley & Sons, Ltd., West Sussex, England, 2003.
[16] J.B. Benziger, M.B. Satterfield, W.H.J. Hogarth, J.P. Nehlsen, I.G. Kevrekidis, J. Power Sources 155 (2) (2006) 272–285.